2016

Development and Validation of a Minichannel Evaporator Model under Different Dehumidifying Conditions

Abdelrahman Hussein Hassan
Institute for Energy Engineering, Universitat Politècnica de València, Spain, abhusab1@upvnet.upv.es

José Gonzálvez-Maciá
Institute for Energy Engineering, Universitat Politècnica de València, Spain, jgonzalv@ter.upv.es

Santiago Martínez-Ballester
Institute for Energy Engineering, Universitat Politècnica de València, Spain, sanmarba@gmail.com

José R. García-Cascales
DITF, ETSII, Universidad Politécnica de Cartagena, Spain, jr.garcia@upct.es

Development and Validation of a Minichannel Evaporator Model under Different Dehumidifying Conditions

Abdelrahman Hussein HASSAN*[1], José GONZÁLVEZ-MACIÁ[1], Santiago MARTÍNEZ-BALLESTER[1], José R. GARCÍA-CASCALES[2]

[1] Universitat Politècnica de València, Institute for Energy Engineering, Camino de Vera, s/n, Valencia, 46022, Spain

[2] Universidad Politécnica de Cartagena, ETSII, DITF, C/ Dr. Fleming, s/n, Cartagena, 30202, Murcia, Spain

*Corresponding Author (Tel: +34963879121, Fax: +34963879126, e-mail: abhusab1@upvnet.upv.es)

ABSTRACT

This paper presents a numerical model (Fin1D-MB) to predict the performance of minichannel evaporators under dehumidifying conditions. The presented model applies a segment-by-segment discretization to the evaporator, adding in each segment a novel bi-dimensional discretization to the fluids flow, fin, and tube wall. The Fin1D-MB model introduces a new approach to model the air-side heat transfer by using a composed function for the fin wall. This function is based on the fundamental one-dimensional fin theory and the technique of movable boundaries between wet and dry portions along the fin height. This modeling scheme allows capturing the heat conduction between tubes and different dehumidifying scenarios for the fin and tube. The proposed model was validated against experimental results for a minichannel evaporator operating with R134a at various test conditions. Generally, the numerical results were in good agreement with the measured data. The predicted inlet refrigerant and outlet air temperatures, refrigerant-side pressure drop, and cooling capacity were within ±0.5 ºC, ±20%, and ±5% error bands, respectively.

1. INTRODUCTION

In order to design a minichannel evaporator quickly and effectively, a reliable simulation tool or numerical model is required. Many minichannel evaporator models are available in the literature, such as Kim and Bullard (2001), Wu and Webb (2002), and Zhao et al. (2012). Most of these neglect the tube-to-tube heat conduction and do not allow for partial dehumidification scenarios. These assumptions simplify the solution, but they result in less freedom to describe the actual processes and phenomena. From our literature review, the only two models which account for the tube-to-tube heat conduction in minichannel evaporators were presented by Ren et al. (2013) and Huang et al. (2015). However, Huang's model also accounts for partial dehumidification scenarios.

Hassan et al. (2015) and (2016) conducted a comparative study of the heat transfer results between a comprehensive two-dimensional numerical model, referred to as Fin2D-W, and the classical ε-NTU approach. The aim of this study was to evaluate the influence of some modeling assumptions on the air-side performance of minichannel evaporators under wet conditions. The results revealed that the assumptions which have the most significant impacts on the heat and mass transfer rates are: the uniform air properties along the fin height, the adiabatic-fin-tip at half the height, and the neglect of partial dehumidification scenarios. These widely used assumptions resulted in substantial deviations in heat transfer results between the ε-NTU approach and Fin2D-W model, especially in the presence of a temperature difference between the adjacent tubes. Nevertheless, the main advantages of the ε-NTU approach are the simplicity and calculation speed, compared to the Fin2D-W model.

These conclusions motivate the authors to develop a simpler model which will be referred to as Fin1D-MB. This model is able to retain the most important heat and mass transfer phenomena as the Fin2D-W model, but with a much lower computational cost. The current work comprises a detailed description of the proposed model and a validation against experimental data for a minichannel evaporator operating with R134a at various test conditions.

2. DEVELOPMENT OF THE FIN1D-MB MODEL

2.1. Evaporator Discretization

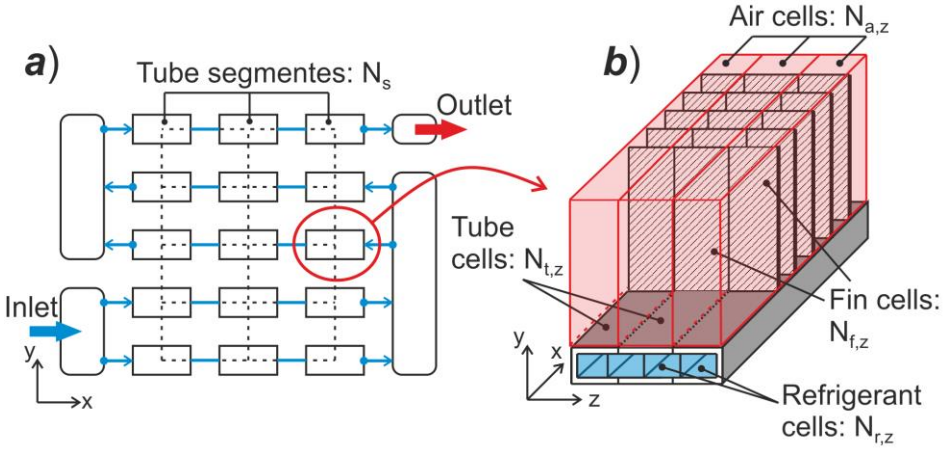

Figure 1: (*a*) Discretization of an evaporator to segments. (*b*) Schematic of a segment discretization into cells.

The model can simulate any refrigerant circuitry arrangement: any number of refrigerant inlets and outlets; and any connection between different tube outlets/inlets at any location. Figure 1*a* shows the discretization of an evaporator to segments, where the dashed lines correspond to the thermal connections between wall cells, whereas the thicker blue lines correspond to the refrigerant flow path. First, the evaporator is discretized along the x-direction (refrigerant flow direction), resulting into N_s segments per tube. Each segment (Figure 1*b*) consists of: a refrigerant flow that is split into $N_{r,z}$ channels in the z-direction (air flow direction); a flat tube which is discretized into $N_{t,z}$ cells in the z-direction; air flow and fins which are always discretized into the same number of cells in the z-direction, where $N_{a,z}=N_{f,z}$. Accordingly, the discretization for an evaporator is summarized in the following as a grid: {N_s, $N_{r,z}$, $N_{t,z}$, $N_{a,z}$}.

2.2. Governing Equations

Every fluid cell (either refrigerant or air) has two nodes, which correspond to the inlet and outlet sections in the fluid flow direction. The tube wall cells have only one node located in the centroid of the cell, as shown in Figure 2. On the other hand, the fins do not have any nodes because a continuous function governs in this case.

2.2.1 Tube wall analysis

The energy conservation equation within any of the tube wall cells *t*, in contact with n_r refrigerant cells, n_a air cells, and n_f fin cells can be written as:

$$\nabla\left(k_t\cdot\nabla T_{c,t}\right)dV+\sum_{r=1}^{n_r}U_{r,t}\left(T_r-T_{c,t}\right)dA_{r,t}+\sum_{a=1}^{n_a}U_{\text{wet},a,t}\left(T_{a,t}^{*}-T_{c,t}\right)dA_{a,t}+\sum_{f=1}^{n_f}dQ_{\text{cond},f}\Big|_{\text{fin root}}=0 \quad (1)$$

It should be noted that a linearization scheme is used in Equation (1) to relate the saturated air humidity ratio to its corresponding surface tube wall temperature (Elmahdy and Biggs, 1983), where $W_{\text{sat},s,t}=a_{a,t}+b_{a,t}\cdot T_{s,t}$.

$T_{c,t}$ is the temperatures evaluated at the centroid of the tube wall cell (°C). k_t and k_f are the thermal conductivity of the tube wall and fin (W/m·K), respectively. $Q_{\text{cond},f}$ is the heat conduction between the tube wall cell and the fin root in contact with it (W). Additionally,

$$U_{r,t}=1/\left[\left(t_t/2\cdot k_t\right)+\left(1/\alpha_{r,t}\right)\right]$$

is the overall heat transfer coefficient for the refrigerant-side (W/m^2·K), where t_t is the wall thickness of tube cell (m), $\alpha_{r,t}$ is the sensible heat transfer coefficient between the refrigerant and tube wall cell (W/m^2·K);

$U_{\text{wet},a,t} = 1/\left[\left(t_t/2\cdot k_t\right)+\left(1/\alpha_{\text{wet},a,t}\right)\right]$ is the overall heat transfer coefficient for the air-side under wet conditions (W/m^2·K);

$\alpha_{\text{wet},a,t} = \alpha_{a,t}\left(1+\beta_a\cdot b_{a,t}\right)$, is the total heat transfer coefficient for the air-side under wet conditions (W/m^2·K), while $\alpha_{a,t}$ is the sensible heat transfer coefficient between the surrounding air and tube wall cell (W/m^2·K), h_{fg} is the latent heat of water condensation (J/kg);

$\beta_a = h_{fg}/C_{p,ma}\cdot Le^{2/3}\,(\text{K})$

$b_{a,t} = \left(W_a - W_{\text{sat},s,t}\right)/\left(T_{dp} - T_{s,t}\right)$ is the slope of saturated humidity ratio line (1/K), as it was defined by Sharqawy and Zubair (2008); and

$T^*_{a,t} = \dfrac{T_a + \beta_a\left[W_a - \left(W_{\text{sat},s,t} - b_{a,t}\cdot T_{s,t}\right)\right]}{1+\beta_a\cdot b_{a,t}}$ is the modified temperature for moist air (°C).

T_a, W_a, T_{dp}, and $C_{p,ma}$ are the moist air temperature (°C), humidity ratio (kg$_{wv}$/kg$_{da}$), dew point temperature (°C), and specific heat (J/kg·K), respectively. T_r is the refrigerant temperature (°C). $T_{s,t}$ and $W_{\text{sat},s,t}$ are the tube wall surface temperature (°C) and saturated humidity ratio evaluated at the surface (kg$_{wv}$/kg$_{da}$), respectively. *Le* is the Lewis number.

2.2.2 Fin wall analysis

The physical discretization of the fin is one-dimensional. However, to capture the actual fin condition, it has to be virtually discretized into three portions (fp1, fp2, and fp3) in the y-direction (along the fin height), as it can be seen in Figure 2*a*. The area of each portion is specified depending on ζ_1 and ζ_2 (m), which represent the boundaries between wet and dry portions. These virtual boundaries are movable from one fin cell to another depending on the fin tip and base temperatures (T_{fT} and T_{fB}) and dew point of surrounding air. According to the previous discussion, each fin cell has a composed governing equation (Equation 2) which consists of three sub-functions. These sub-functions present a continuous temperature profile for the entire fin under any dehumidifying condition.

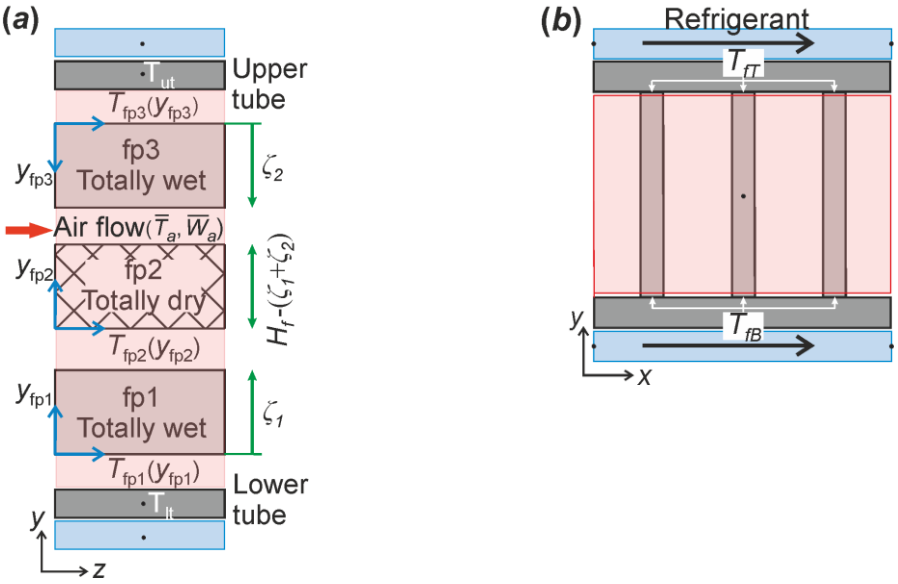

Figure 2: (*a*) Virtual discretization of the fin in y-direction. (*b*) Locations of T_{fB} and T_{fT}.

$$\theta_{a,f}(y)\begin{cases}\theta_{a,\text{fp1}}(y_{\text{fp1}}) = C_1e^{My_{\text{fp1}}} + C_2e^{-My_{\text{fp1}}} - \psi & 0\le y_{\text{fp1}}\le\zeta_1\\ \theta_{a,\text{fp2}}(y_{\text{fp2}}) = C_3e^{my_{\text{fp2}}} + C_4e^{-my_{\text{fp2}}} & 0\le y_{\text{fp2}}\le H_f-(\zeta_1+\zeta_2)\\ \theta_{a,\text{fp3}}(y_{\text{fp3}}) = C_5e^{My_{\text{fp3}}} + C_6e^{-My_{\text{fp3}}} - \psi & 0\le y_{\text{fp3}}\le\zeta_2\end{cases}$$

where $m = \sqrt{P_f\alpha_{a,f}/k_fA_{c,f}}$, $M = m\sqrt{1+\beta_ab_{a,f}}$, and $\psi = \dfrac{\beta_a\left\{W_a - \left[W_{\text{sat},f} - \left(b_{a,f}T_f\right)\right] - b_{a,f}T_a\right\}}{1+\beta_ab_{a,f}}$. (2)

where $\theta_{a,f}$ (K) is the difference between surrounding air temperature T_a and fin temperature T_f, ψ is a parameter which includes the effect of moist air humidity ratio on the fin temperature profile (K), and H_f is the total fin height

(m). $b_{a,f}$ can be calculated as it has been explained in Equation (1), but T_f is used instead of $T_{s,t}$. The boundary conditions that are used to evaluate the unknown constants C_1, C_2, C_3, C_4, C_5, and C_6 are:

$$\text{B.C.}\begin{Bmatrix} \theta_{a,\text{fp1}}(y_{\text{fp1}}=0)=\theta_{a,fB}=T_a-T_{fB};\ \theta_{a,\text{fp1}}(y_{\text{fp1}}=\zeta_1)=\theta_{a,\text{fp2}}(y_{\text{fp2}}=0);\ d\theta_{a,\text{fp1}}/dy_{\text{fp1}}\big|_{y_{\text{fp1}}=\zeta_1}=d\theta_{a,\text{fp2}}/dy_{\text{fp2}}\big|_{y_{\text{fp2}}=0}; \\ \theta_{a,\text{fp3}}(y_{\text{fp3}}=0)=\theta_{a,fT}=T_a-T_{fT};\ \theta_{a,\text{fp2}}\left(y_{\text{fp2}}=H_f-\zeta_1-\zeta_2\right)=\theta_{a,\text{fp3}}(y_{\text{fp3}}=\zeta_2);\ \text{and} \\ d\theta_{a,\text{fp2}}/dy_{\text{fp2}}\big|_{y_{\text{fp2}}=H_f-\zeta_1-\zeta_2}=-d\theta_{a,\text{fp3}}/dy_{\text{fp3}}\big|_{y_{\text{fp3}}=\zeta_2} \end{Bmatrix} \quad (3)$$

Equation (2) and its boundary conditions assume uniform air temperature and humidity ratio along y-direction within the air cell in contact with the evaluated fin cell. So, $\bar{T}_a$ and $\bar{W}_a$ represent the integrated mean values for air temperature and humidity ratio within the cell, respectively. The locations of T_{fB} and T_{fT} are illustrated in Figure 2*b*. In this way, it is possible to define the fin temperature as follows.

$$T_f(y)=\begin{Bmatrix} T_{\text{fp1}}(y_{\text{fp1}})=\bar{T}_a-\theta_{a,\text{fp1}}(y_{\text{fp1}}) \\ T_{\text{fp2}}(y_{\text{fp2}})=\bar{T}_a-\theta_{a,\text{fp2}}(y_{\text{fp2}}) \\ T_{\text{fp3}}(y_{\text{fp3}})=\bar{T}_a-\theta_{a,\text{fp3}}(y_{\text{fp3}}) \end{Bmatrix}_f=\left[A\left(y_{\text{fp1}},y_{\text{fp2}},y_{\text{fp3}}\right)\right]\cdot\begin{bmatrix}\bar{T}_a\\ T_{fB}\\ T_{fT}\\ \bar{\psi}\end{bmatrix} \quad (4)$$

where T_{fp1}, T_{fp2}, and T_{fp3} are the first, second and third fin portion temperatures (°C), respectively. $A(y_{\text{fp1}},y_{\text{fp2}},y_{\text{fp3}})$ is a 3×4 matrix that depends on the local coordinates, fin geometry, m, M, ζ_1, and ζ_2.

2.2.3 Refrigerant analysis

The energy balance in each refrigerant cell r in contact with n_t tube wall cells (t=1—n_t) is explained in Equation (5).

$$\dot{m}_r\cdot dh_r=-\sum_{t=1}^{n_t}\alpha_{r,t}\left(T_r-T_{s,t}\right)dA_{r,t} \quad (5)$$

where h_r and $\dot{m}_r$ are the refrigerant enthalpy (J/kg) and mass flow rate (kg/s), respectively.

The total refrigerant-side pressure drop along the x-direction consists of frictional, acceleration, and gravitational pressure drop terms

$$\left(\frac{dp}{dx}\right)_{r,\text{tot}}=\left(\frac{dp}{dx}\right)_{r,\text{fric}}+\left(\frac{dp}{dx}\right)_{r,\text{acc}}+\left(\frac{dp}{dx}\right)_{r,\text{grav}} \quad (6)$$

In the superheat region, the single-phase total pressure drop can be expressed as:

$$\left(\frac{dp}{dx}\right)_{sp,\text{tot}}=\frac{f_G}{2}\frac{\text{G}_r^2}{D_h\cdot\rho_G}\bigg|_{sp,\text{fric}}+\text{G}_r^2\left[\frac{1}{\rho_G^{\text{out}}}-\frac{1}{\rho_G^{\text{in}}}\right]\bigg|_{sp,\text{acc}}+g\rho_G\sin\xi\big|_{sp,\text{grav}} \quad (7)$$

where G_r is the refrigerant mass flux (kg/m^2·s), D_h is the hydraulic diameter (m), ξ is the tube orientation (deg), and ρ_G is the refrigerant gas density (kg/m^3).

However, in the two-phase region, the total pressure drop for refrigerant-side can be expressed as:

$$\left(\frac{dp}{dx}\right)_{tp,\text{tot}}=\text{G}_r^2\frac{f_L\left(1-\dot{x}\right)^2}{2D_h\cdot\rho_L}\Phi_L^2\bigg|_{tp,\text{fric}}+\text{G}_r^2\frac{d}{dx}\left(\frac{\dot{x}^2}{\rho_G\cdot\varepsilon}+\frac{\left(1-\dot{x}\right)^2}{\rho_G\left(1-\dot{x}\right)}\right)\bigg|_{tp,\text{acc}}+g\left[\varepsilon\rho_G+\left(1-\varepsilon\right)\rho_L\right]\sin\xi\big|_{tp,\text{grav}} \quad (8)$$

where $\dot{x}$ is the vapor quality and ρ_L is the refrigerant liquid density (kg/m^3). Φ_L^2 is the two-phase multiplier based on liquid-phase flow, as it was defined by Mishima and Hibiki (1996). The void fraction ε is modeled as a separated-flow, adopting Chisholm's (1972) correlation for the slip ratio. The correlations employed to evaluate the

refrigerant-side heat transfer coefficient and frictional pressure drop are listed in Table 1.

2.2.4 Moist air analysis

Equation (9) represents the heat rate balance within an air cell *a* in contact with a fin cell *f*, which is discretized into three portions (fp=1─3), and n_t tube cells.

$$\dot{m}_a \cdot C_{p,ma} \cdot dT_a = -\sum_{\mathrm{fp}=1}^{3} \alpha_{a,\mathrm{fp}} \cdot \theta_{a,\mathrm{fp}} \cdot dz dy_{\mathrm{fp}} - \sum_{t=1}^{n_t} \alpha_{a,t} \left(T_a - T_{s,t}\right) dA_{a,t} \tag{9}$$

where $\dot{m}_a$ is the mass flow rate of air (kg/s), while $\theta_{a,\mathrm{fp}}$ (K) and $\alpha_{a,\mathrm{fp}}$ (W/m^2·K) are the temperature difference and sensible heat transfer coefficient between the air and adjacent fin portion, respectively.

The mass balance, taking into account the Chilton-Colburn analogy (Sharqawy and Zubair, 2008), within any air cell gives:

$$\dot{m}_a \cdot dW_a = \frac{1}{Le^{2/3} \cdot C_{p,ma}} \left[-\sum_{\mathrm{fp}=1}^{3} \alpha_{a,\mathrm{fp}} \left(W_a - W_{\mathrm{sat,fp}}\right) \cdot dz dy_{\mathrm{fp}} - \sum_{t=1}^{n_t} \alpha_{a,t} \left(W_a - W_{\mathrm{sat},s,t}\right) dA_{a,t} \right] \tag{10}$$

where $W_{\mathrm{sat,fp}}$ is the saturated air humidity ratio evaluated at the fin portion temperature (kg_{wv}/kg_{da}).

The total air-side pressure drop along the z-direction consists of frictional, acceleration, contraction, and expansion pressure drop terms

$$\left(\frac{dp}{dz}\right)_{a,\mathrm{tot}} = \left(\frac{dp}{dz}\right)_{a,\mathrm{fric}} + \left(\frac{dp}{dz}\right)_{a,\mathrm{acc}} + \left(\frac{dp}{dz}\right)_{a,\mathrm{cont}} + \left(\frac{dp}{dz}\right)_{a,\mathrm{exp}} \tag{11}$$

where the frictional and acceleration terms are calculated similarly to Equations (7). The pressure drop terms due to the sudden contraction and expansion in the heat exchanger are obtained following Kays and London (1984). The different correlations used to evaluate the air-side heat transfer and frictional pressure drop coefficients are shown in Table 1.

In order to discretize the presented governing equations, the finite volume method (FVM) has been applied. In the governing equations, the wall temperature has been considered as the iterative variable of the problem and the semi-explicit method for wall temperature linked equations (SEWTLE), which was proposed by Corberán et al. (2001), has been adopted to solve the problem.

Table 1: Correlations used in the Fin1D-MB model for coefficients evaluation.

Fluid type	Heat transfer coefficient (α)	Frictional pressure drop	Expansion/Contraction pressure losses
Refrigerant:			
Single-phase region	Gnielinski (1976)	Churchill (1977)	Kays and London (1984)
Two-phase region	Kandlikar and Balasubramanian (2004)	Mishima and Hibiki (1996)	Kays and London (1984)
Air:			
Dry condition	Kim and Bullard (2002a)	Kim and Bullard (2002a)	Kays and London (1984)
Wet condition	Kim and Bullard (2002b)	Kim and Bullard (2002b)	Kays and London (1984)

2.3. Solution Methodology

After the initialization process, the iterative procedure begins, which consists of three main steps. The first step is to calculate the outlet air temperature and humidity ratio (Equations 9 and 10), and outlet refrigerant enthalpy (Equation 5) for all fluids cells. In the first iteration the dehumidifying conditions of the fins have not yet been evaluated, so all the fins are assumed to be totally dry (ζ_1= ζ_2=0). The second step is to calculate the tube wall cells' temperatures using Equation (1). It can be observed that this equation considers the 2D heat conduction between the current tube cell and adjacent cells, which results in a system of linear equations involving all the tube cells temperatures. To solve this system of equations, the line-by-line iteration method (Patankar, 1980) is adopted in the current model.

The final step of the iterative procedure is to evaluate the dehumidifying condition of each fin cell (either to be totally dry, totally wet, or partially wet) then to calculate its average temperature. Firstly, the fin cell dehumidifying condition is evaluated according to the fin cell root temperatures, average dew point temperature of the surrounding air, and the predicted temperature profile of the fin. After identifying the real fin cell condition, the following equations are applied to calculate the exact length for each fin portion:

$$\zeta_1 = \frac{1}{m}\cdot\ln\left\{-\frac{1}{2\left(\theta_{a,fT}e^{mH_f}-\theta_{a,fB}\right)}\left[-\bar{\theta}_{dp}e^{3mH_f}+\bar{\theta}_{dp}e^{mH_f}+\sqrt{\begin{matrix}\bar{\theta}_{dp}^2e^{6mH_f}-2\left(2\theta_{a,fB}\theta_{a,fT}e^{mH_f}+\bar{\theta}_{dp}^2-2\theta_{a,fB}^2\right)e^{4mH_f}\\+\left(4\theta_{a,fT}^2e^{2mH_f}-4\theta_{a,fB}\theta_{a,fT}e^{mH_f}+\bar{\theta}_{dp}^2\right)e^{2mH_f}\end{matrix}}\right]e^{-mH_f}\right\} \quad (12)$$

$$\zeta_2 = H_f-\left\{\frac{1}{m}\cdot\ln\left[\frac{1}{2\left(\theta_{a,fT}e^{mH_f}-\theta_{a,fB}\right)}\left(\bar{\theta}_{dp}e^{3mH_f}-\bar{\theta}_{dp}e^{mH_f}+\sqrt{\begin{matrix}\bar{\theta}_{dp}^2e^{6mH_f}-2\left(2\theta_{a,fB}\theta_{a,fT}e^{mH_f}+\bar{\theta}_{dp}^2-2\theta_{a,fB}^2\right)e^{4mH_f}\\+\left(4\theta_{a,fT}^2e^{2mH_f}-4\theta_{a,fB}\theta_{a,fT}e^{mH_f}+\bar{\theta}_{dp}^2\right)e^{2mH_f}\end{matrix}}\right)e^{-mH_f}\right]\right\} \quad (13)$$

where $\bar{\theta}_{dp}=\bar{T}_a-\bar{T}_{dp}$, $\theta_{a,fB}=\bar{T}_a-T_{fB}$, and $\theta_{a,fT}=\bar{T}_a-T_{fT}$.

Finally, ζ_1 and ζ_2 are used to determine the average fin cell temperature (Equation 4). It can be noted that the calculation process of obtaining the fin wall temperature field is explicit. The iterative process continues until the value of the residual converges to the required tolerance.

3. EXPERIMENTAL SETUP

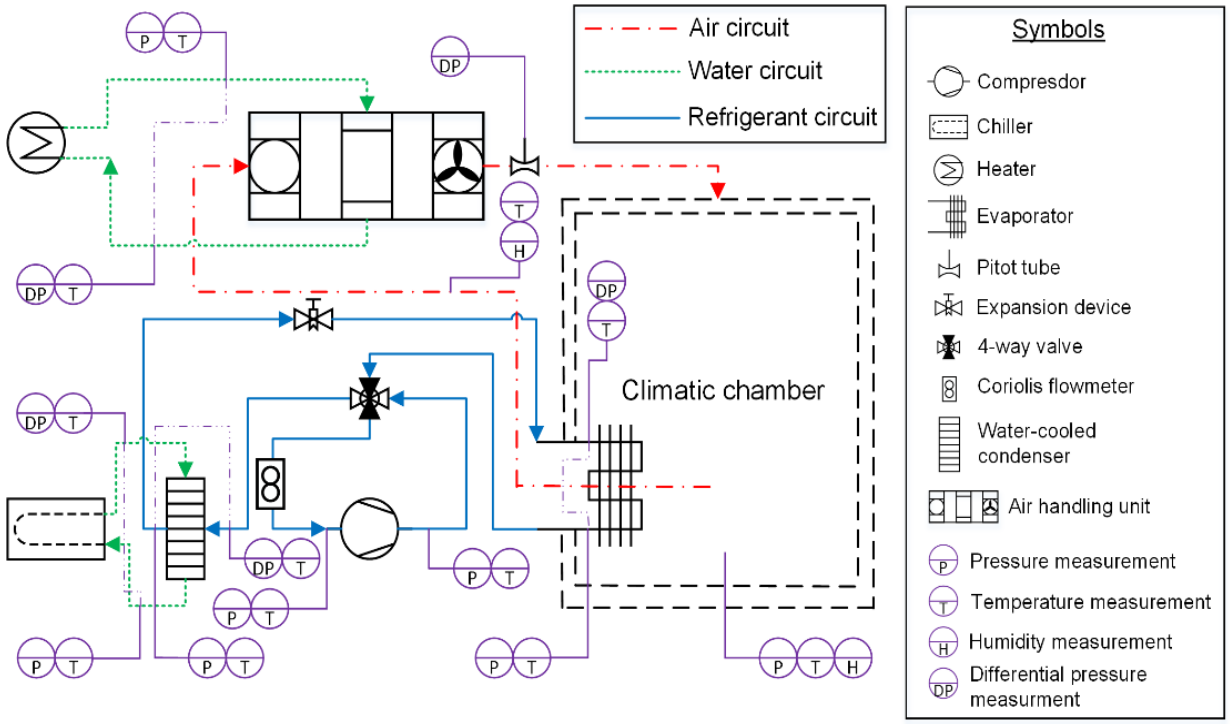

Figure 3: Schematic diagram of the test facility.

The experiments were carried out in a reversible air-to-refrigerant heat pump test facility, as shown in Figure 3, which mainly consists of three circuits: air, water, and refrigerant loops. The heat pump operates with R134a and it is equipped with: a multi-speed hermetic reciprocating compressor with a displacement of 34.38 cm^3, a brazed plate condenser (water-to-refrigerant), and an electronic valve as the expansion device.

The tested evaporator is a single slap minichannel heat exchanger, which was provided by Modine Co. It is 340 mm high, 483 mm wide, and 21.1 mm thick. It comprises 33 multiport flat tubes, which are arranged in four paths (8–6–7–12). Regarding the refrigerant-side, the tube is characterized by eight triangular ports having a hydraulic diameter equal to 0.78 mm. The fins are louvered type with a density equal to 14 fin/inch. Table 2 shows the operating conditions which were specified as input data for the tested evaporator.

The uncertainties for pressure, temperature, mass flow rate, compressor power, and compressor speed measurements were about ±0.15%, ±0.3 °C, ±0.1%, ±0.5%, and ±0.1 Hz, respectively. The energy balance between the air-side and refrigerant-side was within ±5%.

Table 2: Operating conditions for the R134a minichannel evaporator.

Air		**Refrigerant**	
Inlet dry-bulb temperature (°C)	7	Inlet mass flow rate (kg/h)	32.4─38
Inlet relative humidity (%)	73─89	Inlet vapor quality (-)	0.22─0.24
Inlet flow rate (m^3/h)	890─1890	Outlet superheat (K)	7.9─12.6

4. MODEL VALIDATION

After developing the Fin1D-MB model, it has been integrated into the IMST-ART® simulation program (IMST-ART, 2010) to allow evaluating the performance of entire evaporator. The IMST-ART® program has been developed by the Institute for Energy Engineering, Technical University of Valencia (UPV). This program is capable of simulating any refrigerant circuit; additionally, it can evaluate the performance of individual refrigeration components.

The validation of the proposed model was conducted using the experimental data as described in Section 3. The numerical grid size chosen was the one that gave a good balance between accuracy and computational cost. According to the definition given in Sub-section 2.1, the grid employed for all the predicted results was: {5,3,3,3}.

The inputs to the model were refrigerant superheat, inlet vapor quality, inlet air temperature and relative humidity, and inlet mass flow rate of refrigerant and air. Whereas, inlet refrigerant temperature, refrigerant-side pressure drop, outlet air temperature, and cooling capacity were the selected parameters to validate the Fin1D-MB model. Figures 4─7 compare simulation results with the experimental data. It can be seen in Figures 4 that the current model predicts the inlet refrigerant temperatures $T_{r,in}$ within ±0.5 °C error bands. The mean absolute error (MAE) and standard deviation (SD) of the predicted values are ±0.24 °C and ±0.25 °C, respectively.

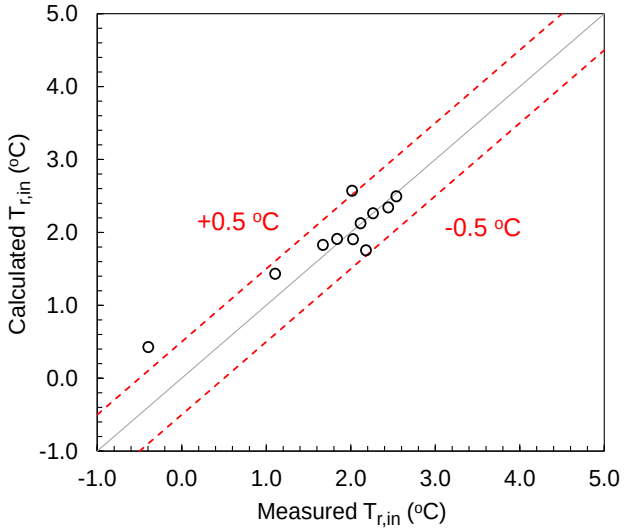

Figure 4: Comparison of the inlet refrigerant temperature $T_{r,in}$ between the calculated and measured values.

Figure 5 presents the calculated refrigerant-side pressure drop Δp_r against the measured data. The proposed model successively estimates the Δp_r within ±20% error bands, with MAE and SD values of ±9.12% and ±7.18%, respectively. Although, the MAE and SD of the predicted Δp_r are relatively high, it was found that their effect on the evaporator capacity was rather small.

Regarding the air-side, Figure 6 shows the calculated outlet air temperature $T_{a,out}$ values versus the measured ones. It can be observed that approximately all the predicted values are within ±0.5 ºC error bands, with MAE and SD of ±0.43 ºC and ±0.34 ºC, respectively.

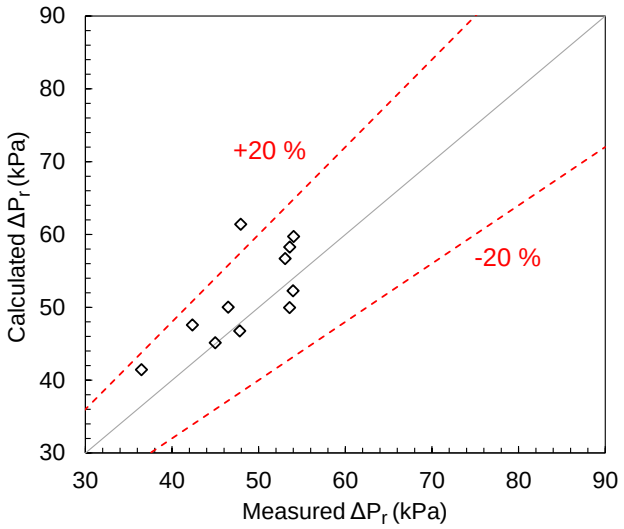

Figure 5: Comparison of the refrigerant-side pressure drop Δp_r between the calculated and measured values.

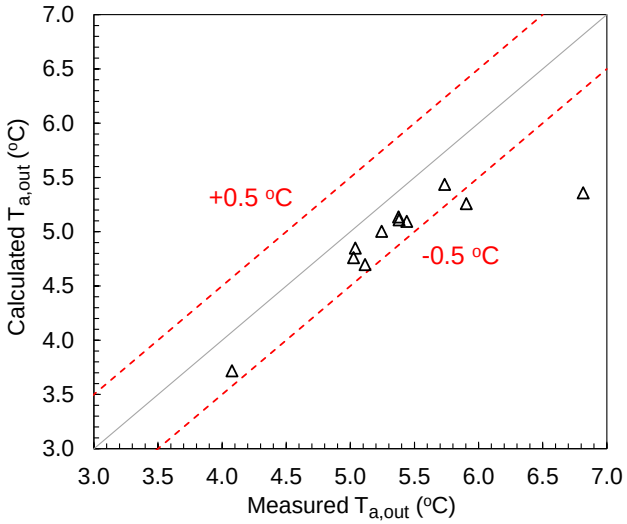

Figure 6: Calculated vs. measured outlet air temperature, $T_{a,out}$.

The good prediction of the refrigerant and air temperatures has a positive impact on the estimated cooling capacity Q_r, as shown in Figure 7. The Fin1D-MB model can predict the cooling capacity with good agreement, with MAE and SD of ±1.8% and ±0.3%, respectively. For the current study, no adjustment factors were applied either to the heat transfer or frictional pressure drop coefficients.

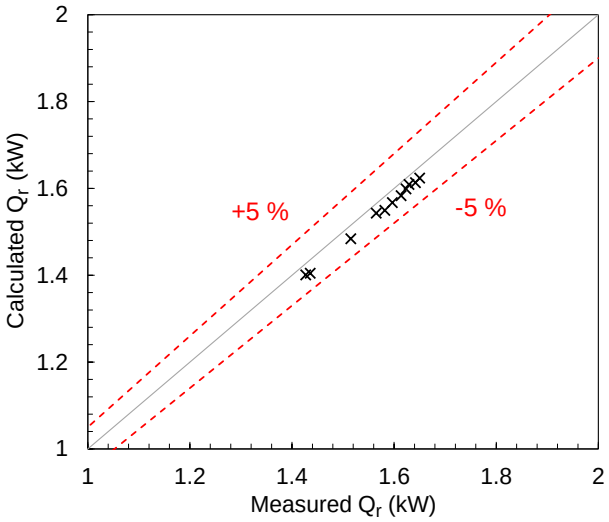

Figure 7: Calculated vs. measured cooling capacity, Q_r.

5. CONCLUSIONS

A one-dimensional numerical model (Fin1D-MB) for minichannel evaporators was presented. The Fin1D-MB model is based on the fundamental fin theory in conjunction with the moving boundaries technique for the air-side. This innovative scheme substantially reduces the discretization complexity and computation time. Additionally, it allows capturing different dehumidifying scenarios and tube-to-tube heat conduction. After developing the Fin1D-MB model, it was validated against experimental data for R134a evaporator under different operating conditions. The proposed model predicted the outlet air temperate within ±0.5 ºC error bands with a MAE of ±0.43 ºC. Regarding the refrigerant-side, the Fin1D-MB model successfully estimated the inlet refrigerant temperature within error bands of ±0.5 ºC with a MAE of ±0.24 ºC, the pressure drop within error bands of ±20% with a MAE of ±9.12%, and the cooling capacity within error bands of ±5% with a MAE of ±1.8%.

NOMENCLATURE

α	heat transfer coefficient (W/m^2·K)
A	contact area (m^2)
A_c	cross-section area (m^2)
f	Darcy–Weisbach friction factor
g	gravitational acceleration (m/s^2)
M	wet fin parameter (1/m)
m	dry fin parameter (1/m)
P	perimeter (m)
V	volume (m^3)
x,y,z	spatial coordinates (m)

Subscript/Superscript

a	air, air cell index
c	centroid
dp	dew point
f	fin, fin cell index
fB	fin base
fT	fin tip
fp1, fp2, fp3	fin portions
G	gas
in	inlet
L	liquid
out	outlet
r	refrigerant, refrigerant cell index
s	surface
sat	saturated
sp	single-phase
t	tube, tube cell index
tot	total
tp	two-pahse

REFERENCES

Chisholm, D., 1972, an Equation for Velocity Ratio in Two-Phase Flow, *NEL Report 535*.
Churchill, S., 1977, Friction-factor Equation Spans all Fluid Flow Regimes, *Chem. Eng.*, vol. 7: p. 91-92.
Corberán, J.M., De-Cordoba, P.F., Gonzálvez-Macia, J., Alias, F., 2001, Semiexplicit Method for Wall Temperature Linked Equations (SEWTLE): a General Finite-volume Technique for the Calculation of Complex Heat Exchangers, *Numer. Heat Tr. B-Fund.*, vol. 40, no. 1: p. 37-59.
Elmahdy, A.H., Biggs, R.C., 1983, Efficiency of Extended Surfaces with Simultaneous Heat Transfer and Mass Transfer, *ASHRAE J.*, vol. 89: p. 135-143.
Gnielinski, V., 1976, New Equations for Heat and Mass Transfer in Turbulent Pipe and Channel Flow, *Int. Chem. Eng.*, vol. 16, no. 2: p. 359-368.
Hassan, A.H., Martinez-Ballester, S., Gonzálvez-Maciá, J., 2015, a Comparative Study between a Two-dimensional Numerical Minichannel Evaporator Model and a Classical Effectiveness-NTU Approach under Different Dehumidifying Conditions, *Sci. Technol. Built Environ*, vol. 21, no. 5: p. 681-692.
Hassan, A.H., Martínez-Ballester, S., Gonzálvez-Maciá, J., 2016, Two-dimensional Numerical Modeling for the Air-side of Minichannel Evaporators Accounting for Partial Dehumidification Scenarios and Tube-to-tube Heat Conduction, *Int. J. Refrig.*, vol. 67: p. 90-101.
Huang, L., Bacellar, D., Aute, V., Radermacher, R., 2015, Variable Geometry Microchannel Heat Exchanger Modeling under Dry, Wet and Partially Wet Surface Conditions Accounting for Tube-to-tube Heat Conduction, *Sci. Technol. Built Environ*, vol. 21, no. 5: p. 703-717.
IMST-ART, 2010, *Simulation Tool to Assist the Selection, Design and Optimization of Refrigeration Equipment and Components*, Instituto de Ingeniería Energética, Universitat Politècnica de València, Spain. Online at: http://www.imst-art.com.
Kandlikar, S., Balasubramanian, P., 2004, an Extension of the Flow Boiling Correlation to Transition, Laminar, and Deep Laminar Flows in Minichannels and Microchannels, *Heat Transfer Eng.*, vol. 25: p. 86-93.
Kays, W.M., London, A.L., 1984, *Compact Heat Exchangers*, 3rd ed., McGraw-Hill, New York, NY.
Kim, M.-H., Bullard, C., 2001, Development of a Microchannel Evaporator Model for a CO_2 Air-conditioning System, *Energy*, vol. 26: p. 931-948.
Kim, M.-H., Bullard, C., 2002a, Air-side Thermal Hydraulic Performance of Multi-louvered Fin Aluminum Heat Exchangers, *Int. J. Refrig.*, vol. 25: p. 390-400.
Kim, M.-H., Bullard, C., 2002b, Air-side Performance of Brazed Aluminum Heat Exchangers under Dehumidifying Conditions, *Int. J. Refrig.*, vol. 25: p. 924-934.
Mishima, K., Hibiki, T., 1996, Some Characteristics of Air-water Two-phase Flow in Small Diameter Vertical Tubes, *Int. J. Multiphas Flow*, vol. 22: p. 703-712.
Patankar, S.V., 1980, *Numerical Heat Transfer and Fluid Flow*, Hemisphere, New York, NY.
Ren, T., Ding, G., Wang, T., Hu, H., 2013, a General Three-dimensional Simulation Approach for Micro-channel Heat Exchanger Based on Graph Theory, *Appl. Therm. Eng.*, vol. 59: p. 660-674.
Sharqawy, M.H., Zubair, S.M., 2008, Efficiency and Optimization of Straight Fins with Combined Heat and Mass Transfer – an Analytical Solution, *Appl. Therm. Eng.*, vol. 28: p. 2279-2288.
Wu, X.M., Webb, R.L., 2002, Thermal and Hydraulic Analysis of a Brazed Aluminum Evaporator, *Appl. Therm. Eng.*, vol. 22: p. 1369-1390.
Zhao, Y., Liang, Y., Sun, Y., Chen, J., 2012, Development of a Mini-channel Evaporator Model Using R1234yf as Working Fluid, *Int. J. Refrig*., vol. 35: p. 2166-2178.

ACKNOWLEDGEMENT

Abdelrahman Hussein Hassan, is partially supported by the FPI scholarship (sub-program 2, 2015) which has been provided by the Universitat Politècnica de València (UPV). Financial support from the Spanish Ministry of Economy and Finance (project number: DPI2011-26771-C02-01) is also gratefully acknowledged.